

GT2017-64631

**DRAFT: DESIGN OF A CENTRIFUGAL COMPRESSOR STAGE AND A
RADIAL-INFLOW TURBINE STAGE FOR A SUPERCRITICAL CO₂
RECOMPRESSION BRAYTON CYCLE BY USING 3D INVERSE DESIGN METHOD**

Jiangnan Zhang

Advanced Design Technology Ltd
Dilke House
1 Malet Street
London, WC1E 7JN
UK
Email: jz@adtechnology.co.uk

Pedro Gomes

Advanced Design Technology Ltd
Dilke House
1 Malet Street
London, WC1E 7JN
UK
Email: pg@adtechnology.co.uk

Mehrdad Zangeneh

Department of Mechanical Engineering
University College London
Gower Street
London, WC1E 6BT
UK
Email: m.zangeneh@ucl.ac.uk

Benjamin Choo

Advanced Design Technology Ltd
Dilke House
1 Malet Street
London, WC1E 7JN
UK
Email: bc@adtechnology.co.uk

ABSTRACT

It is found that the ideal gas assumption is not proper for the design of turbomachinery blades using supercritical CO₂ (S-CO₂) as working fluid especially near the critical point. Therefore, the inverse design method which has been successfully applied to the ideal gas is extended to applications for real gas by using a real gas property look up table. A fast interpolation look up approach is implemented which can be applied both in superheated and two phase regimes. This method is applied to the design of a centrifugal compressor blade and a radial-inflow turbine blade for a S-CO₂ recompression Brayton cycle. The stage aerodynamic performance (volute included) of the compressor and turbine is validated numerically by using the commercial CFD code ANSYS CFX R162. The structural integrity of the design is also confirmed by using ANSYS Workbench Mechanical R162.

NOMENCLATURE

Roman Symbols

c_P specific heat capacity at constant pressure, $J/(kg \times K)$
 h specific enthalpy, kJ/kg
 \dot{m} mass flow rate, kg/s
 r radial coordinate, m
 s specific entropy, $kJ/(kg \times K)$
 x dryness fraction
 z axial coordinate, m
 H_0^* rothalpy, kJ
 P pressure, Pa or MPa
 R radius, mm
 T temperature, K
 T_0^* rotary total temperature, K
 V_θ tangential velocity, m/s
 \dot{W} power, W
 \vec{W} relative velocity vector, m/s

Greek Symbols

η	efficiency
ρ	density, kg/m^3
τ	torque, $N \times m$
ω	rotating speed, rad/s
Ω	rotating speed, rad/s

Superscripts

* rotary properties

Subscripts

0	total or stagnation
1	inlet
2	outlet
<i>g</i>	gas
<i>h</i>	constant specific enthalpy
<i>hub</i>	hub
<i>is</i>	isentropic
<i>l</i>	liquid
<i>s</i>	constant specific entropy
<i>shr</i>	shroud
<i>t - s</i>	total-to-static
<i>t - t</i>	total-to-total
<i>HTR</i>	high temperature recuperator
<i>LE</i>	leading edge
<i>LTR</i>	low temperature recuperator
<i>MC</i>	main compressor
<i>RC</i>	recompressing compressor
<i>TE</i>	trailing edge

Abbreviations

ER	expansion ratio
CFD	computational fluid dynamics
FEA	finite element analysis
HTR	high temperature recuperator
LMTD	log mean temperature difference
LTR	low temperature recuperator
MC	main compressor
NIST	National Institute of Standards and Technology
PC	pre-cooler
PR	pressure ratio
RC	recompressing compressor
RGP	real gas property
RIT	radial-inflow turbine
S-CO ₂	supercritical carbon dioxide

INTRODUCTION

The supercritical cycle which always operates above the critical pressure and critical temperature of its working fluid was devised to overcome disadvantages of Rankine cycle and recuperated Brayton cycle and retain their advantages by Feher in the 1960s [1]. Feher compared critical temperature and pressure of eight different working fluids which can be used in practical supercritical cycle applications and CO₂ was selected as the most suitable working fluid for the following reasons: 1) its moderate critical pressure (7.38 MPa) allows lower cycle operating pressure; 2) its thermal stability and chemical inertness are very high within the temperature range of interest [2]; 3) its abundance, non-toxicity and low cost. Another advantage of S-CO₂ which was pointed out by Dostal [3] is that its low critical temperature (31°C) makes it is suitable to be used in non-condensing cycles for high efficiency since the maximum temperature difference can be achieved. A series of study by Angelino [4–6] showed that reheat CO₂ cycles have higher efficiency, simpler layout and smaller prime mover (gas turbine) within turbine inlet temperature range of 650 - 1000°C compared to double reheat steam cycle. Dostal [3] compared several different compound Brayton cycles and concluded that the recompression cycle has the simplest layout and achieves the highest efficiency at operating condition of turbine inlet pressure ~ 20 MPa and turbine inlet temperature of 550°C among all the studied cycles. In a detailed review of current S-CO₂ power cycle technology, Ahn et al. [7] investigated the performance of six different single flow cycle layouts and six different split flow cycle layouts. It is found that the recompression cycle layout shows the best efficiency ($\sim 44\%$ for turbine inlet temperature of 500 °C) but requires the largest recuperator size which is assessed by Log Mean Temperature Difference (LMTD) method.

Moore et al. [8] developed a 1 MW S-CO₂ test loop to measure the mechanical and flow performance of costumed turbine expander and recuperator at Southwest Research Institute. Cho et al. [9] from Korea Institute of Energy Research tested two S-CO₂ cycles (10 kW and 1 kW). The turbo-generator was unable to operate stably due to the very high rotating speed (200,000 RPM). The development of a 60 kW test loop using the axial impulse turbine is ongoing. Wang et al. [10] from Nuclear Power Institute of China presented some preliminary results on the design of a Integral Test Loop of MW scale S-CO₂ power cycles. They are planning to build a 10 MW Integral Test Loop before 2020.

To maximize S-CO₂ cycle efficiency, more and more attention have been paid into aerodynamic design and optimization of compressors and turbines operating with S-CO₂ by using 1D meanline analysis and three-dimensional CFD.

Monje et al. [11] proposed a detailed 1D design strategy for S-CO₂ compressors and average values of compressor inlet and outlet temperature and pressure from the CFD calculation (ANSYS FLUENT) showed good agreement with the 1D model. Qi

et al. [12] coupled the S-CO₂ real gas property table with different loss models proposed by Moustapha et al. [13] in their 1D in-house code TOPGEN and applied it in the preliminary design of S-CO₂ radial turbines. Lee et al. [14] compared three different methods of converting static (temperature and pressure) to stagnation values in the 1D meanline S-CO₂ compressor design. It was concluded that the real gas isentropic exponents method provides better conversion results than the ideal gas based method but the conversion error near the critical point is still non-negligible. Shao et al. [15] applied a design parameter called velocity ratio at the impeller inlet (IVR) to control the condensation zone near the S-CO₂ compressor leading edge.

Pecnik et al. [16] performed a 3D CFD study of a S-CO₂ compressor impeller and CFD results showed that calculated ideal head coefficient and efficiency are higher than experimental data [17] [18] which can be explained by the simplified model used in the simulation. Shroud tip clearance and vaned diffuser are not modelled and therefore the rotating shroud will add extra momentum to the flow. Rinaldi et al. [19] improved this numerical model by including shroud tip clearance gap and vaned diffuser blade in the simulation. The relative difference between calculated efficiency and experimental efficiency was reduced from 16% to 4%. Baltadjiev et al. [20] used commercial software ANSYS CFX to investigate real gas effects in S-CO₂ centrifugal compressors mainly near critical point. Zhao et al. designed a S-CO₂ centrifugal compressor [21] and investigated the influence of tip clearance on S-CO₂ compressor performance [22]. Zhang et al. [23] performed a numerical study on a 15 MW S-CO₂ axial turbine and 1.5 MW S-CO₂ radial turbine using commercial software NUMECA. Ameli et al. [24] presented a steady numerical study of a S-CO₂ compressor. The efficiency and pressure ratio values obtained from CFD (ANSYS CFX) using a RGP (real gas property) table with sufficient resolution match experimental results very well (less than 2% error).

Long term exposure to high pressure and high temperature S-CO₂ of different components in the S-CO₂ Brayton cycle may cause serious corrosion problem. The CO₂ corrosion behaviour of different materials has been widely studied for different pressure and temperature range. Rouillard et al. [25] performed an experimental comparison of corrosion behaviour of different steels in S-CO₂ at 550°C and 25 MPa and found that austenitic alloys are much more corrosion resistant than ferritic-martensitic steel. Wright et al. [26] discussed unique materials requirements of different components (turbine, compressor and heat exchanger) in the S-CO₂ closed and open cycles. Sridharan et al. [27] investigated the corrosion performance of a number of high temperature alloys in supercritical CO₂ (650°C and 21 MPa) environment. The most CO₂ corrosion resistant materials are PM 2000, PE16, Haynes 230 and INCONEL Alloy 625.

In this paper a design study of S-CO₂ compressor and radial turbine used in a recompression Brayton cycle using 3D inverse design method is presented. For the first time, the real gas effect

is implemented in the inverse design and is validated by comparing the blade loading (blade surface static pressure) from 3D inviscid inverse design and 3D viscous CFD simulation. The aerodynamic performance and flow field of the compressor and the turbine are investigated by CFD and their structural strength is evaluated by static structural analysis.

A S-CO₂ RECOMPRESSION BRAYTON CYCLE

A S-CO₂ recompression Brayton cycle is proposed based on Sarkar's analysis [28] and its layout is shown in Fig. 1. CO₂ is assumed to be always working in the supercritical region which makes the minimum cycle temperature and minimum cycle pressure limited by critical values. Sarkar's study shows that as CO₂ approaches critical point the cycle becomes more efficient due to two reasons: 1) the compression work needed is less (higher CO₂ density); 2) increased heat transfer in the recuperator caused by higher c_p value. In the literature, the minimum cycle temperature is selected to be 304-310 K to maximize the cycle efficiency. However, it is also widely reported that the very low cycle temperature will result in a condensation area near the compressor LE. The compressor efficiency will be very poor when its inlet flow is in the two-phase region according to Poerner et al. [29]. It is also found that CFD (ANSYS CFX) becomes very difficult to converge for the given temperature range above. Therefore, the minimum cycle temperature and pressure are selected as 320 K and 7.6 MPa to ensure that CO₂ always works in the supercritical region.

The maximum cycle temperature is controlled by the reactor and increasing its value can result in higher net thermal efficiency. The upper value of temperature is limited to a moderate value of 800 K to avoid any possible strength and corrosion problems for the radial-inflow turbine. The maximum cycle pressure is set as 15.2 MPa by assuming the pressure ratio (PR) of compressors is 2.0. The flow is split into two parts at point 9: 75% for MC (main compressor) and 25% for RC (recompressing compressor).

INVERSE DESIGN METHOD WITH REAL GAS

The inverse design method used in this paper is a three-dimensional inviscid compressible method. The basic governing equation of this method are based on a kinematic approach involving solution of potential flow equations with Clebsch-Monge formulation to represent rotational effects and described by Zangeneh [30]. The blade geometry is computed iteratively based on the prescribed rV_θ distribution and meridional shape, where V_θ is the circumferentially averaged tangential velocity. This method is also known as Circulation method and available as a commercial code TURBOdesign1 [31].

This code was initially implemented only for turbomachines working with ideal gas. From Fig. 2 it can be seen that the com-

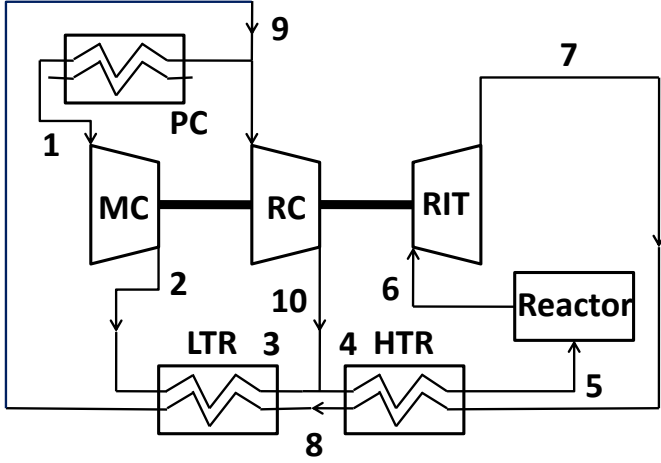


FIGURE 1. LAYOUT OF S-CO₂ RECOMPRESSION BRAYTON CYCLE FOR A NUCLEAR REACTOR

compressibility factor of CO₂ is very low near the critical temperature and the ideal gas assumption does not hold any more. Therefore, the real gas effect is brought into inverse design method by employing a look up table on the basis of RGP (Real Gas Property) files. Previously ideal gas assumption is used to compute the density based on the calculated velocity field through the Eqn. (1). The term in bracket represents the temperature ratio $\frac{T}{T_0^*}$, where ω is the rotational speed, \vec{W} is the relative velocity vector and T_0^* is the rotary total temperature. For the real gas case this equation becomes the original rothalpy equation (see Eqn. (2)) since c_p is not constant any more. In Eqn. (2) H_0^* is the rothalpy which can be calculated based on inlet boundary conditions and remains constant throughout the flow domain in an inviscid flow. Once the velocity field (\vec{W}) is known, the static enthalpy h can be computed by Eqn. (2). Static entropy s is also constant which can be obtained from inlet boundary conditions since the flow is assumed to be isentropic. h and s are then used in the look up table to find corresponding pressure, temperature and density.

$$\frac{\rho}{\rho_0^*} = \left(1 + \frac{\omega^2 r^2 - \vec{W} \cdot \vec{W}}{2c_p T_0^*} \right)^{1/(\gamma-1)} \quad (1)$$

$$\frac{h}{H_0^*} = 1 + \frac{\omega^2 r^2 - \vec{W} \cdot \vec{W}}{2H_0^*} \quad (2)$$

In a RGP file, the data is stored in such a way that given pressure and temperature, all other thermodynamics properties

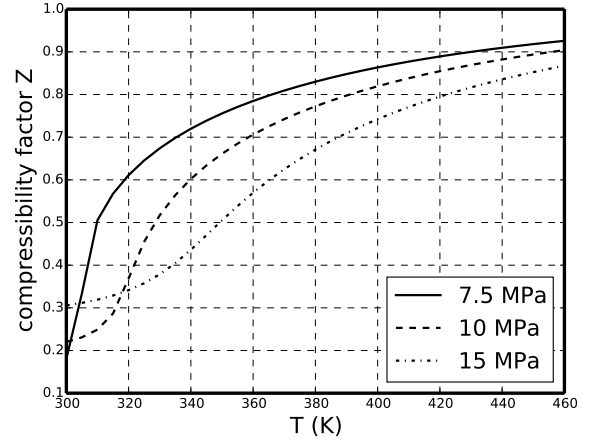


FIGURE 2. CO₂ COMPRESSIBILITY FACTOR

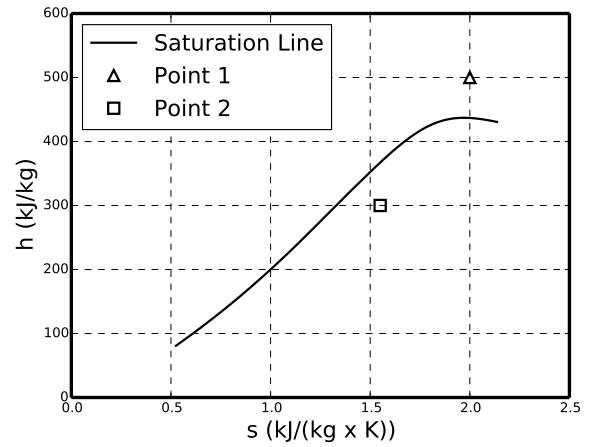


FIGURE 3. SATURATION LINE ON CO₂ h-s DIAGRAM

can be found by direct interpolation of the table. In the inverse design method described above, h and s are known. Therefore, a reversed interpolation of RGP tables is required to find other thermodynamic properties based on known h and s . The first step is to compare given h and s with saturation line on the h-s diagram (see example Fig. 3) to determine which table will be used for the reversed interpolation.

Reversed Interpolation in Superheated Table

If given h and s fall in the superheated region (Point 1 in Fig. 3), for each pressure level in the superheated table, temperature is searched which has the same value of h and s . Two curves with constant h and s with respect to P and T can be generated as

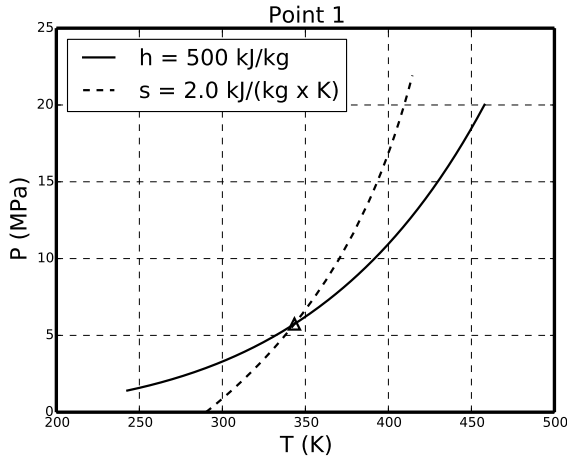


FIGURE 4. CONSTANT h AND s CURVES ON CO_2 P-T DIAGRAM

shown in Fig. 4. The intersection of these two curves will give the required P and T .

Reversed Interpolation in Saturation Table

If given h and s fall in the two phase region ((Point 2 in Fig. 3), the procedure becomes more complicated since there is dryness fraction x in the thermodynamic state. For each pressure level in the saturation table, dryness fraction for constant enthalpy x_h and for constant entropy x_s are calculated based on Eqn. (3) and (4). Two curves with constant h and s with respect to P and x can be generated as shown in Fig. 5. The intersection of these two curves will give the required P and x .

$$x_h = \frac{h - h_l}{h_g - h_l} \quad (3)$$

$$x_s = \frac{s - s_l}{s_g - s_l} \quad (4)$$

This method is validated by comparing the blade loading (blade surface static pressure distribution) obtained from the inverse design and 3D CFD simulation at three different spanwise locations for the main compressor. The hub and mid span blade loading from inviscid inverse design code match with CFD results quite well which can be seen in Fig. 6 and Fig. 7. In Fig. 8 the pressure on the pressure surface where $m > 0.2$ and on the suction surface where $m > 0.4$ are slightly overestimated. The reason for this discrepancy is that the tip clearance effect near

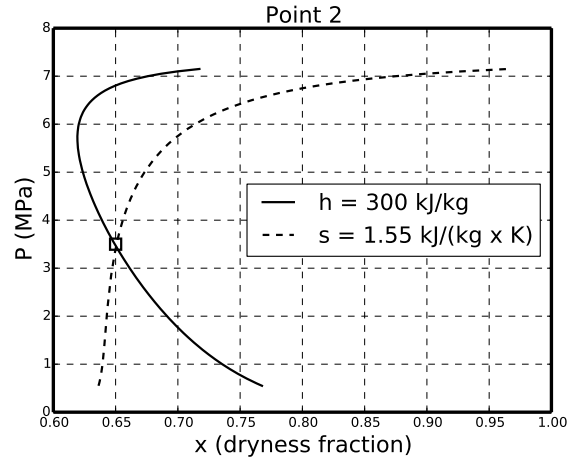


FIGURE 5. CONSTANT h AND s CURVES ON CO_2 P-x DIAGRAM

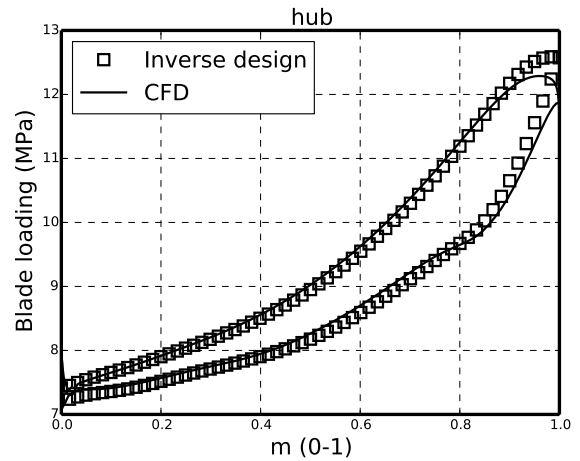


FIGURE 6. COMPARISON OF HUB BLADE LOADING CALCULATED USING INVERSE DESIGN AND CFD

the shroud is not modelled in the inverse design method. An improved matching can be seen in Fig. 9 by removing the tip clearance in the CFD.

BLADE GENERATION AND VOLUTE DESIGN

Meridional Geometry and Blade Thickness

Compressor and turbine meridional geometries are obtained by using design specifications in Table 1 as input to 1D mean-line code TURBODesign Pre [32] with a CO_2 RGP file. The meridional shapes are shown in Fig. 10 and Fig. 11. Meridional dimensions are summarised in Table 2 and Table 3. The hub

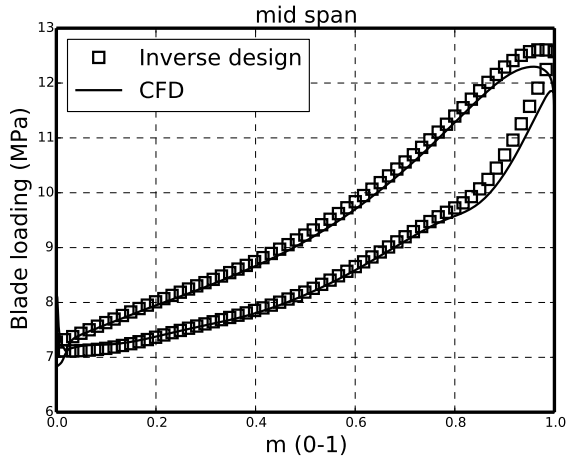


FIGURE 7. COMPARISON OF MID SPAN BLADE LOADING CALCULATED USING INVERSE DESIGN AND CFD

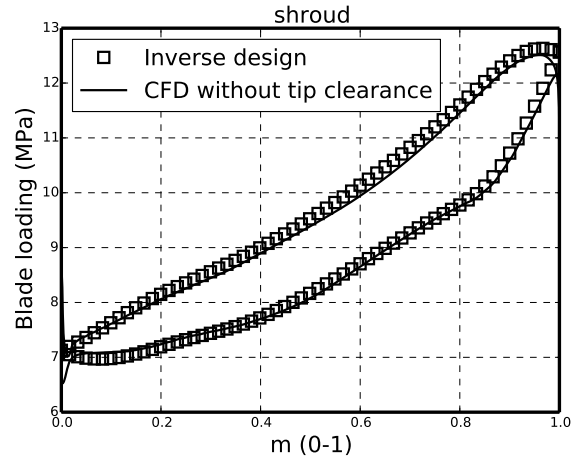


FIGURE 9. COMPARISON OF SHROUD BLADE LOADING CALCULATED USING INVERSE DESIGN AND CFD EXCLUDING TIP CLEARANCE

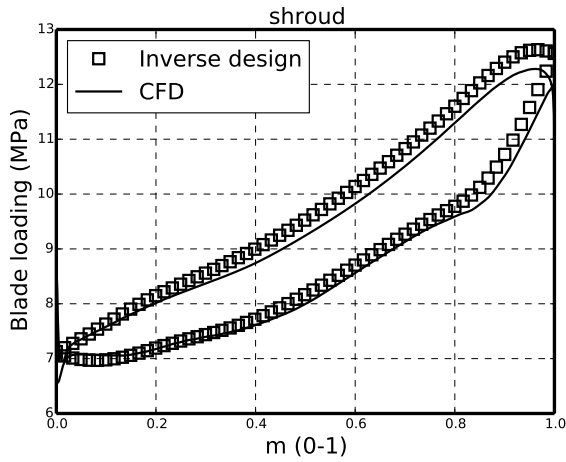


FIGURE 8. COMPARISON OF SHROUD BLADE LOADING CALCULATED USING INVERSE DESIGN AND CFD

thickness of the compressor blade is set as 3 mm constant and the shroud thickness is set as 1 mm constant. The turbine blade thickness is using a profile distribution at the hub and a constant of 1 mm at the shroud. The thickness between hub and shroud is calculated through linear interpolation.

Blade Loading

Blade loading used in the inverse design method is defined as $\frac{drV_\theta}{dm}$, where m is the meridional distance. Three segment method used to define the blade loading is illustrated by Zangeneh et al. [33]. Two points NC and ND divide the loading

TABLE 1. DESIGN SPECIFICATION OF S-CO₂ COMPRESSOR AND TURBINE

	MC	RIT
P_{01} (MPa)	7.6	15.2
T_{01} (K)	320	800
PR_{t-t} / ER_{t-t}	2.0	2.0
RPM (rev/min)	14,000	14,000
\dot{m} (kg/s)	131.25	175

curve into three separated parts. First and third parts are parabolic and middle part is a straight line with given slope ($SLOPE$). The loading value at LE is specified by $DRVT$. rV_θ at the blade LE and TE are chosen based on Euler Turbomachinery Equation (Eqn. (5)). rV_θ distribution in the meridional channel can be obtained through interpolation and integration based on blade loading at hub and shroud. The blade loading used for the compressor blade is shown in Fig. 12. Aft-loaded hub is used to prevent the low momentum flow near hub LE and aft-loaded shroud is used to reduce the maximum Mach number near shroud TE. Aft-loaded hub and shroud can also be seen from the blade surface static pressure plots (Fig. 6 and Fig. 8). The blade geometry is computed iteratively based on the prescribed meridional shape,

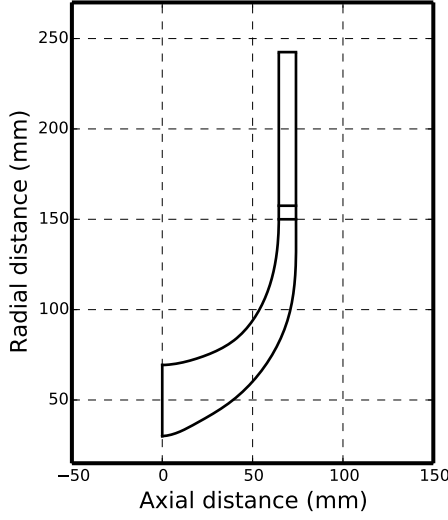


FIGURE 10. MERIDIONAL GEOMETRY OF MC IMPELLER AND DIFFUSER

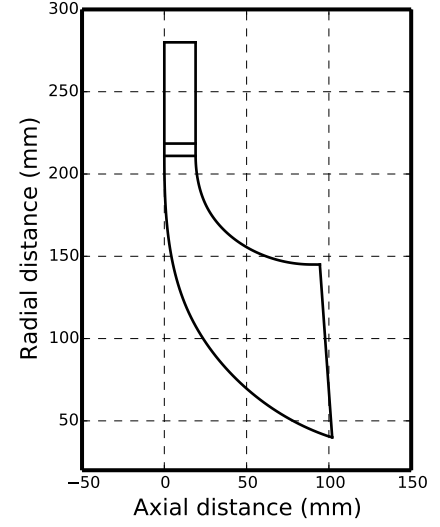


FIGURE 11. MERIDIONAL GEOMETRY OF TURBINE NOZZLE AND IMPELLER

TABLE 2. COMPRESSOR MERIDIONAL DIMENSIONS

impeller $R_{LE,hub}$ (mm)	30
impeller $R_{LE,shr}$ (mm)	69.34
impeller R_{TE} (mm)	150
impeller W_{tip} (mm)	9.5
impeller L (mm)	74
number of impeller blades	14
diffuser R_{LE} (mm)	157.5
diffuser R_{TE} (mm)	242.5
number of diffuser blades	13

TABLE 3. TURBINE MERIDIONAL DIMENSIONS

nozzle R_{LE} (mm)	280
nozzle R_{TE} (mm)	218.5
number of nozzle blades	16
impeller W_{tip} (mm)	19
impeller R_{LE} (mm)	211
impeller $R_{TE,hub}$ (mm)	40
impeller $R_{TE,shr}$ (mm)	145
impeller L (mm)	102
impeller α_{TE}	4°
number of impeller blades	11

blade thickness distribution and blade loading.

$$\frac{\tau}{\dot{m}} = (rV_{\theta})_{LE} - (rV_{\theta})_{TE} \quad (5)$$

Volute design

Compressor and turbine volutes are designed using commercial software TURBObdesign Volute [34] which is a 2D inverse design code. A number of different volute cross-section shapes

including circular, elliptic, rectangular and trapezoidal can be selected. It is also necessary to specify some basic volute geometrical dimensions such as volute inlet/outlet radius and width. In this paper both compressor and turbine volutes are designed to be symmetric with a circular cross-section shape. The volute cross-section area at different spiral angles are calculated iteratively based on specified radial and tangential velocities at the volute outlet/inlet which can be obtained from CFD results. The volute geometry is constructed by lofting all the calculated cross-

TABLE 4. FOUR LEVELS OF COMPRESSOR GRIDS

impeller	diffuser	volute	No. of elements
280,645	254,558	741,056	1,276,259
372,332	343,434	1,016,022	1,731,788
602,020	544,600	1,607,655	2,754,275
1,193,626	1,079,364	3,167,100	5,440,090

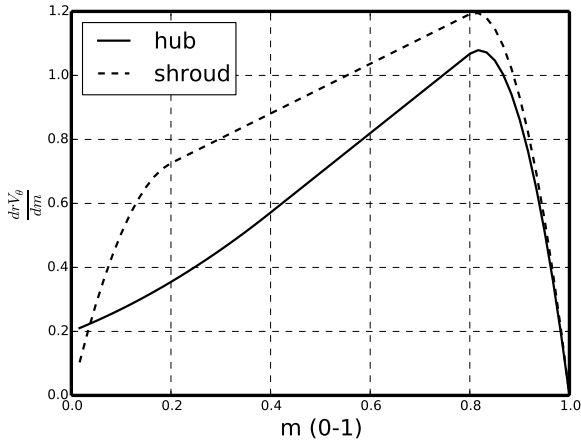


FIGURE 12. MC BLADE LOADING DISTRIBUTION

section areas. A compressor volute can be seen in Fig. 13 which has been meshed.

STEADY CFD SIMULATION

Steady CFD simulation is performed by using commercial software ANSYS CFX R162.

Mesh Generation and Mesh Dependency Analysis

ANSYS TurboGrid R162 is used to generate structured mesh for impeller and diffuser (or nozzle) as shown in Fig. 13. There is 20 layers of grid in the shroud clearance and constant clearance of 0.3 mm is applied for both compressor and turbine impellers. The volute geometries are meshed using ANSYS Workbench Meshing Tool R162.

A mesh dependency analysis is performed by comparing normalised compressor total-to-total pressure ratio (PR_{t-t}) and isentropic total-to-total efficiency η_{t-t} for different levels of grids (Table 4 and Fig. 14). The mesh level with around 2,700,000 elements is selected based on the consideration of the

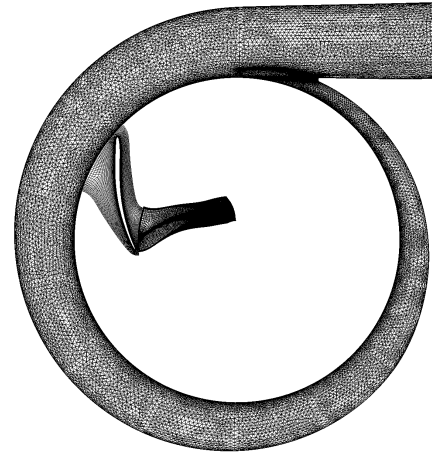


FIGURE 13. MC CFD COMPUTATIONAL MESH

accuracy and computational cost.

Boundary Conditions

Inlet boundary conditions are total pressure and total temperature. Inlet flow direction is normal to the inlet boundary. Outlet boundary condition is mass flow rate. The impeller is rotating at a constant speed of 14,000 rev/min. Turbulence model is chosen as SST $k - \omega$ [35]. The interface type between impeller and diffuser /nozzle or diffuser/nozzle and volute is set as stage (mixing plane). Periodic boundary condition is also applied on the periodic surfaces. CFX solver found it is very difficult to converge without any initialization. Therefore, the outlet mass flow rate and impeller RPM is gradually increased from a small value and the CFD results are used as initialization step by step until the correct mass flow and RPM are reached.

RGP Table Dependency Analysis

CO₂ RGP file (or table) is used in the ANSYS CFX to model S-CO₂ properties. RGP file can be generated based on data from a commercial software NIST REFPROP V9.1. The CO₂ equation of state (EOS) used to calculate all properties is from [36]. In the RGP file, fluid properties are stored with the structure of different temperature and pressure. The temperature and pressure range used is 300 K to 900 K and 5 MPa to 18 MPa. To assess the effect of interpolation and numerical error which may be introduced by different size of RGP files, three different RGP files are used for CFD calculation with same mesh and results are summarised in Table 5. It can be concluded that the error brought by different RGP files can be neglected.

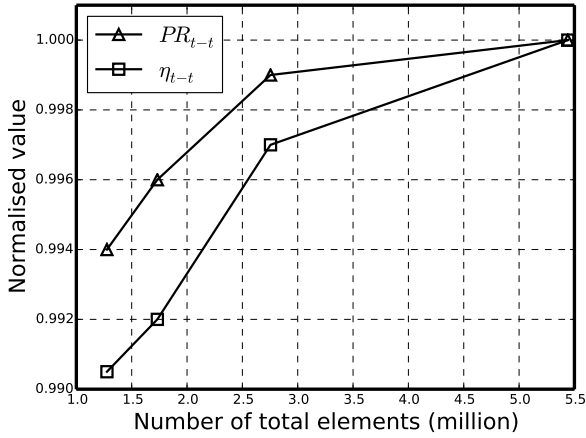


FIGURE 14. MESH DEPENDENCY ANALYSIS

TABLE 5. RGP TABLE DEPENDENCY ANALYSIS

	RGP 1	RGP 2	RGP 3
ΔT (K)	6	2	0.9
ΔP (kPa)	65	26	13
PR_{t-t}	2.024	2.018	2.018
η_{t-t} (%)	91.07	90.93	90.92

Flow Field Analysis

Figure 15, Figure 16 and Figure 17 show the relative velocity vector plots of the compressor blades at three different spanwise locations. It can be seen that the flow attached the blade very well and there is no obvious flow separation. There is a few secondary flow near the shroud TE which is caused by the tip leakage flow near the impeller tip.

From Fig. 6 and Fig. 8 it can be seen that the blade hub and shroud are aft-loaded as we have specified in Fig. 12. Figure 18 shows the rV_θ^* meridional contour from inverse design method and CFD. rV_θ^* is rV_θ non-dimensionalised by blade tip radius (R_{tip}) times blade tip speed (U_{tip}) and defined by Eqn. (6). Spanwise rV_θ^* distribution in the inverse design method is purely linear which is obtained by linear interpolation of hub and shroud rV_θ^* we specified. rV_θ^* from CFD in the inducer part is very close to values in the inverse design since the flow velocity is low and tip leakage flow is negligible. When the flow is developing from the inducer to the exducer, the discrepancy between CFD rV_θ^* and inverse design rV_θ^* is growing. One possible explanation is that the end wall effect caused by the flow viscosity becomes more dominant while the inverse design method is inviscid. The

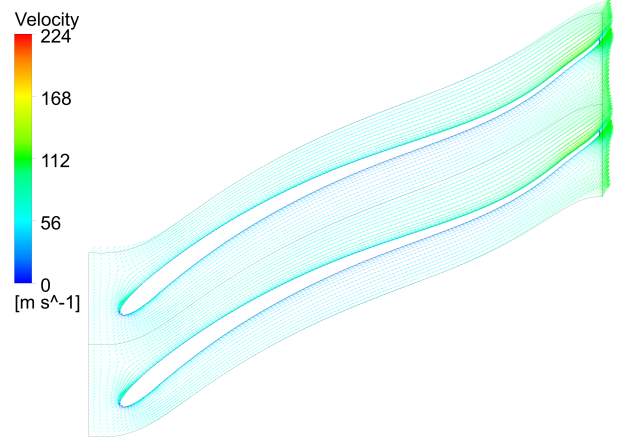


FIGURE 15. RELATIVE VELOCITY VECTOR AT MC HUB

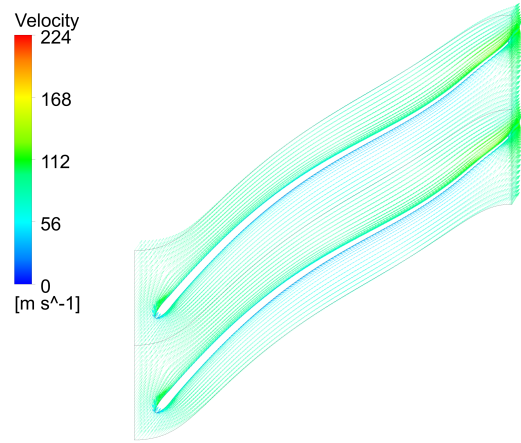


FIGURE 16. RELATIVE VELOCITY VECTOR AT MC MID SPAN

tip leakage flow near is also developing while the inverse design method does not model it.

$$rV_\theta^* = \frac{rV_\theta}{R_{tip}U_{tip}} \quad (6)$$

Turbine isentropic total-to-static efficiency can be expressed by Eqn. (7). To maximize the turbine efficiency at the given design point $(rV_\theta)_{LE}$ needs to be maximised and $(rV_\theta)_{TE}$ needs to be minimised. A CFD rV_θ^* distribution from the nozzle inlet to turbine outlet is shown in Fig. 19. Where station 1 is the nozzle inlet, station 2 is the impeller inlet and station 3 is the impeller outlet. It can be seen that rV_θ^* from the volute outlet entering the nozzle is around 0.36 and is accelerated by the nozzle blade to

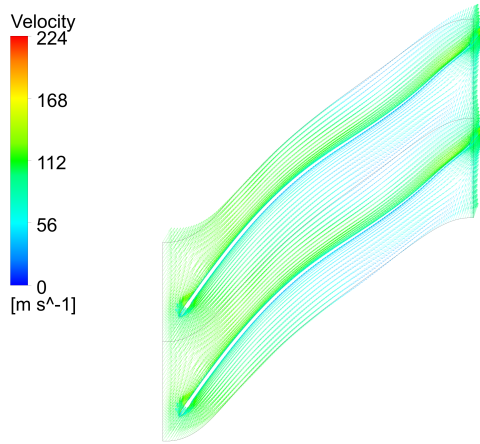


FIGURE 17. RELATIVE VELOCITY VECTOR AT MC SHROUD

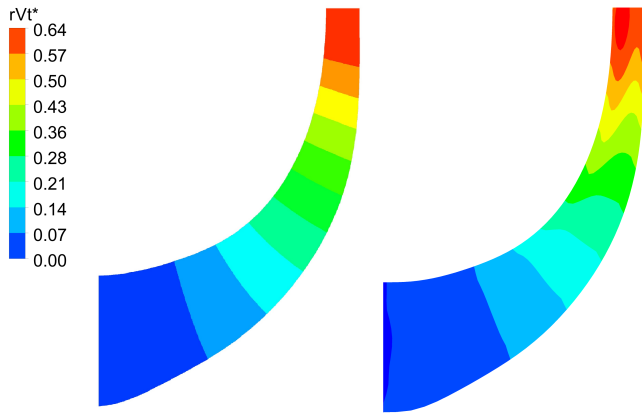


FIGURE 18. COMPARISON OF rV_{θ}^* SPECIFIED IN INVERSE DESIGN METHOD (LEFT) AND CALCULATED FROM CFD (RIGHT)

0.96. All the tangential swirl (velocity) are removed by the impeller blade. Zero rV_{θ}^* at the turbine outlet minimised the kinetic energy loss and gives the high turbine efficiency.

$$\eta_{t-s} = \frac{h_{01} - h_{02}}{h_{01} - h_{2s}} = \frac{\Omega \tau}{\dot{m}(h_{01} - h_{2s})} = \frac{\Omega [(rV_{\theta})_{LE} - (rV_{\theta})_{TE}]}{h_{01} - h_{2s}} \quad (7)$$

CFD results for MC and RIT are summarised in Table 6. Compressor pressure ratio and turbine expansion ratio values are very close to the design specification shown in Table 1. The efficiency of RC (recompressing compressor) will be lower than MC due to the higher inlet temperature. The power consumed by the RC can be approximately estimated as 1.5-2.0 MW. Therefore,

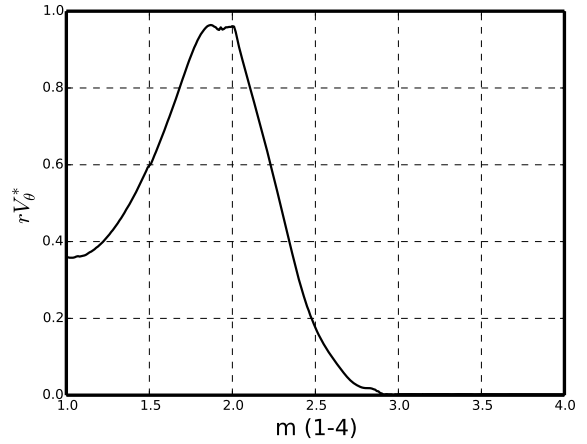


FIGURE 19. AVERAGED rV_{θ}^* FROM NOZZLE INLET TO TURBINE OUTLET

TABLE 6. CFD RESULTS

	MC	RIT
PR_{t-t} / ER_{t-t}	2.02	1.99
\dot{W} (MW)	4.11	15.89
η_{t-t}	90.9%	91.5%
η_{t-s}	-	89.2%

the net power output will be 9.78-10.28 MW. The compressor and turbine stage efficiency are very high but it should be noted that surface roughness, heat transfer loss and total pressure loss in the pipe are not considered in the CFD simulation.

STATIC STRUCTURAL ANALYSIS

To evaluate the mechanical strength of the compressor and turbine impellers, ANSYS Workbench Mechanical R16.2 is used to perform a static structural analysis. The compressor and turbine material is selected based on the comparison of the yield strength of four most CO₂ corrosion resistant materials (PM 2000, INCONEL alloy 625, PE16 and Haynes alloy 230 [27]). From Fig. 20 [37–40] it can be seen that the most suitable material is INCONEL A625 for the maximum temperature up to 800 °C. The material properties of INCONEL A625 is summarised in Table 7 [37]. The density of INCONEL A625 is set a constant value of 8.44 g/cm³.

The unstructured computational mesh for FEA analysis is generated using ANSYS Workbench Meshing Tool and an ex-

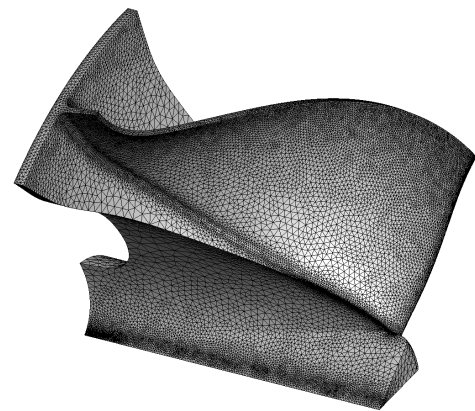
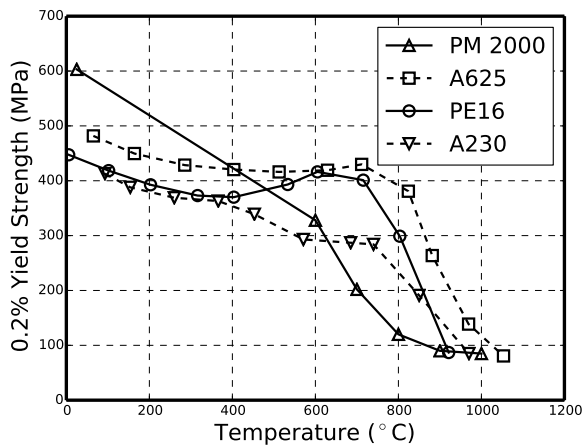
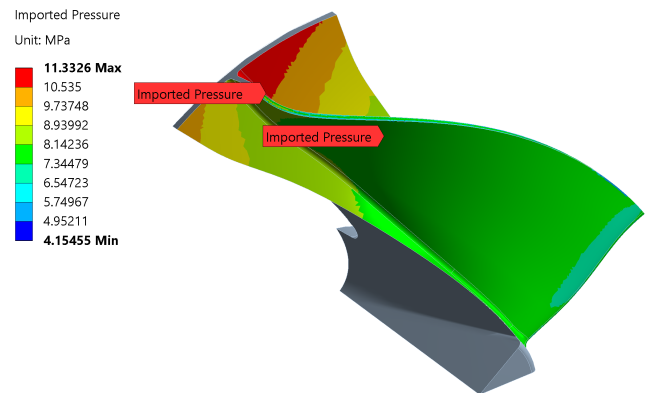


FIGURE 20. COMPARISON OF YIELD STRENGTH AT DIFFERENT TEMPERATURE

FIGURE 21. RIT FEA COMPUTATIONAL MESH

TABLE 7. MATERIAL PROPERTIES OF INCONELL A625 [37]

Temperature (°C)	Coefficient of Thermal Expansion ($\times 10^{-5} \text{ } ^\circ\text{C}^{-1}$)	Young's Modulus (GPa)	Poisson's Ratio (-)
204	1.31	197.9	0.286
316	1.33	191.7	0.290
427	1.37	185.8	0.295
538	1.40	178.6	0.305



ample of RIT mesh is shown in Fig. 21. Only one blade sector is used since the turbine (or compressor) wheel is axisymmetric. The total number of elements used in the analysis is around 400,000.

FIGURE 22. RIT BLADE AND HUB PRESSURE DISTRIBUTION FROM CFD

Two cyclic regions can be defined on the two periodic surfaces to save computational time and cost. The blade is rotating at a speed of 14,000 *rev/min* and a cylindrical support is applied on the shaft. Pressure loading obtained from stage CFD results can be imported and imposed on the impeller hub and blade surfaces (see an example in Fig. 22). The pressure on the impeller backplate and turbine outlet (or compressor inlet) shaft surface also need to be specified which is not available in the CFD simulation. These pressure values are estimated based on turbine/compressor inlet and outlet average static pressures. For RIT the thermal loading has to be taken into account since the CO_2 temperature in the turbine is very high (485 °C in the turbine impeller LE from CFD). However, a conjugate heat transfer

simulation is necessary to get an accurate body temperature distribution of the turbine wheel which is too expensive. A simple model used to approximate the turbine body temperature distribution is proposed and shown in Fig. 23. The maximum and minimum temperature can be calculated from the mass flow averaged static temperature measured at the RIT LE and TE. It is known that the hottest part of the turbine is always in the LE and the temperature of the flow is decreasing along the streamwise direction. Therefore, it is reasonable to assume that the turbine body temperature is decreasing from LE (maximum temperature) to the backplate and TE (minimum temperature). In other word, the turbine body temperature distribution is only a function of z which is the rotational axis coordinate.

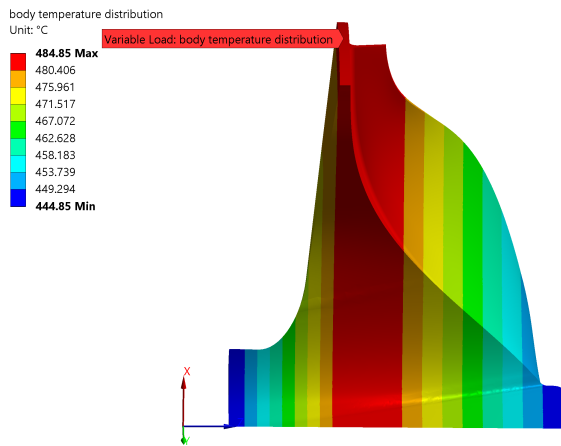


FIGURE 23. ASSUMED TEMPERATURE DISTRIBUTION OF RIT IMPELLER

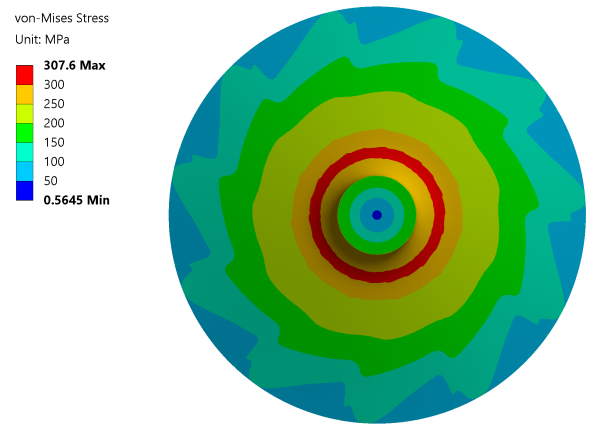


FIGURE 25. von-Mises STRESS CONTOUR AT RIT IMPELLER BACKPLATE

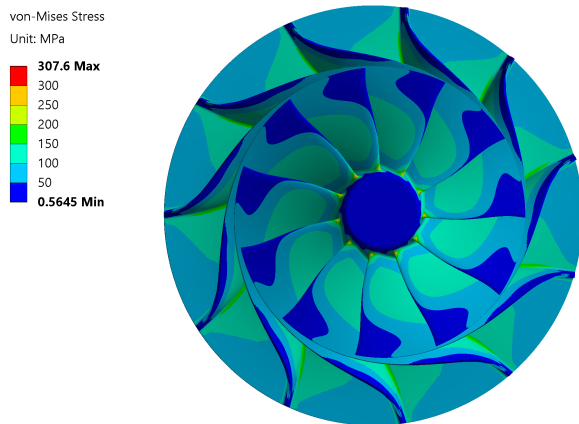


FIGURE 24. von-Mises STRESS CONTOUR AT RIT IMPELLER HUB AND BLADE SURFACE

von-Mises stress contour of RIT wheel are shown in Fig. 24 and Fig. 25. The maximum stress on the blade surface is near the location of hub LE and the maximum stress on the backplate is near the shaft. The maximum stress values for MC and RIT are shown in Table 8 which are all less than the material yield strength 420 MPa.

CONCLUSION

A detailed design procedure of a centrifugal compressor stage and a radial-inflow turbine stage for S-CO₂ recompression Brayton cycle using inverse design is presented in this paper.

TABLE 8. MAXIMUM von-Mises STRESS

	MC	RIT
maximum stress (MPa)	316.0	307.6

Compressor and turbine blades are generated by using 3D inverse design method which is extended from ideal gas to real gas applications through reversed interpolation in the superheated and saturation tables.

Steady CFD results show that both compressor and turbine have very high stage efficiency (90.9%-91.5% total-to-total). There is a very good agreement between blade loading (rV_{θ}^*) specified by inviscid inverse design method and calculated by 3D viscous CFD.

INCONEL A625 is selected as compressor and turbine material with the consideration of corrosion and strength. Both pressure loading and temperature loading from CFD calculation are included in the static structural analysis. Results show that compressor and turbine maximum von-Mises stress does not exceed the limit of yield strength in the working condition.

The design of the recompressing compressor is ongoing.

ACKNOWLEDGMENT

The authors would like to acknowledge Michael Rimmer for his work on the S-CO₂ cycle and initial design of the compressor during his MSc study in the University College London in 2013.

REFERENCES

- [1] Feher, E. G., 1968. “The Supercritical Thermodynamics Power Cycle”. *Energy Conversion*, **8**(2), pp. 85–90.
- [2] Bailey, H. E., 1965. *Equilibrium Thermodynamic Properties of Carbon Dioxide*. NASA SP-3014, Washington, D. C.
- [3] Dostal, V., 2004. “A Supercritical Carbon Dioxide Cycle for Next Generation Nuclear Reactors”. PhD Thesis, Massachusetts Institute of Technology, Cambridge, MA, January. Available from: dspace.mit.edu/handle/1721.1/17746.
- [4] Angelino, G., 1967. “Perspectives for the Liquid Phase Compression Gas Turbine”. *Journal of Engineering for Gas Turbine and Power*, **89**(2), pp. 229–236.
- [5] Angelino, G., 1968. “Carbon Dioxide Condensation Cycles for Power Production”. *Journal of Engineering for Gas Turbine and Power*, **90**(3), pp. 287–295.
- [6] Angelino, G., 1969. “Real Gas Effect in Carbon Dioxide Cycles”. *ASME 1969 Gas Turbine Conference and Products Show*.
- [7] Ahn, Y., Bae, S. J., Kim, M., Cho, S. K., Baik, S., Lee, J. I., and Cha, J. E., 2015. “Review of Supercritical CO₂ Power Cycle Technology and Current Status of Research and Development”. *Nuclear Engineering and Technology*, **47**(6), pp. 647–661.
- [8] Moore, J., Brun, K., Evans, N., Bueno, P., and Kalra, C., 2014. “Development of A 1 MWe Supercritical CO₂ Brayton Cycle Test Loop”. *The 4th International Symposium - Supercritical CO₂ Power Cycles*.
- [9] Cho, J., Shin, H., R., H.-S., Lee, G., Roh, C., Lee, B., and B., Y.-J., 2016. “Development of the Supercritical Carbon Dioxide Power Cycle Experimental Loop in KIER”. *Proceedings of ASME Turbo Expo 2016*, **GT2016-57460**.
- [10] Wang, J., Huang, Y., Zang, J., and Liu, G., 2016. “Preliminary Design and Considerations of A MWe Scale Supercritical CO₂ Integral Test Loop”. *Proceedings of ASME Turbo Expo 2016*, **GT2016-56426**.
- [11] Monje, B., Sánchez, D., M.Savill, Pilidis, P., and Sánchez, T., 2014. “A Design Strategy For Supercritical CO₂ Compressors”. *Proceedings of ASME Turbo Expo 2014*, **GT2014-25151**.
- [12] Qi, J., Reddell, T., Qin, K., Hooman, K., and Jahn, I. H. J., 2016. “Supercritical CO₂ Radial Turbine Design Performance as A Function of Turbine Size Parameters”. *Proceedings of ASME Turbo Expo 2016*, **GT2016-58137**.
- [13] Moustapha, H., Zelesky, M. F., Baines, N. C., and Japikse, D., 2003. *Axial and Radial Turbines*, Vol. 2. Concepts NREC White River Junction, VT.
- [14] Lee, J., Cho, S. K., Cha, J. E., and Lee, J. I., 2016. “Sensitivity Study of S-CO₂ Compressor Design for Different Real Gas Approximations”. *Proceedings of ASME Turbo Expo 2016*, **GT2016-57100**.
- [15] Shao, W., Wang, X., Yang, J., Liu, H., and Huang, Z., 2016. “Design Parameters Exploration for Supercritical CO₂ Centrifugal Compressors under Multiple Constraints”. *Proceedings of ASME Turbo Expo 2016*, **GT2016-56820**.
- [16] Pecnik, R., Rinaldi, E., and Colonna, P., 2012. “Computational Fluid Dynamics of A Radial Compressor Operating with Supercritical CO₂”. *Proceedings of ASME Turbo Expo 2012*, **GT2012-69640**.
- [17] Wright, S. A., Radel, R. F., Vernon, M. E., Rochau, G. E., and Pickard, P. S., 2010. Operation and Analysis of A Supercritical CO₂ Brayton Cycle. SANDIA REPORT SAND2010-0171, Sandia National Laboratories.
- [18] Fuller, R. L., and Eisemann, K., 2011. “Centrifugal Compressor Off-design Performance for Super-critical CO₂ Power Cycle Symposium”. *Supercritical CO₂ Power Cycle Symposium*.
- [19] Rinaldi, E., Pecnik, R., and Colonna, P., 2013. “Steady State CFD Investigation of A Radial Compressor Operating with Supercritical CO₂”. *Proceedings of ASME Turbo Expo 2013*, **GT2013-94580**.
- [20] Baltadjiev, N., Lettieri, C., and Spakovszky, Z., 2014. “An Investigation of Real Gas Effects in Supercritical CO₂ Centrifugal Compressors”. *Proceedings of ASME Turbo Expo 2014*, **GT2014-26180**.
- [21] Zhao, H., Deng, Q., Zheng, K., Zhang, H., and Feng, Z., 2014. “Numerical Investigation on the Flow Characteristics of A Supercritical CO₂ Centrifugal Compressor”. *Proceedings of ASME Turbo Expo 2014*, **GT2014-26646**.
- [22] Zhao, H., Deng, Q., Zhang, H., and Feng, Z., 2015. “The Influence of Tip Clearance on Supercritical CO₂ Centrifugal Compressor Performance”. *Proceedings of ASME Turbo Expo 2015*, **GT2015-42627**.
- [23] Zhang, H., Zhao, H., Deng, Q., and Feng, Z., 2015. “Aerodynamic Design and Numerical Investigation of Supercritical Carbon Dioxide Turbine”. *Proceedings of ASME Turbo Expo 2015*, **GT2015-42619**.
- [24] Ameli, A., Turunen-Saaresti, T., and Backman, J., 2016. “Numerical Investigation of the Flow Behavior Inside A Supercritical CO₂ Centrifugal Compressor”. *Proceedings of ASME Turbo Expo 2016*, **GT2016-57481**.
- [25] Rouillard, F., Charton, F., and Moine, G., 2009. “Corrosion Behavior of Different Metallic Materials in Supercritical CO₂ at 550°C and 250 bars”. *Proceedings of SCCO₂ Power Cycle Symposium 2009*.
- [26] Wright, I. G., Ping, B. A., Shingledecker, J. P., and Thimsen, D., 2013. “Materials Considerations for Supercritical CO₂ Turbine Cycles”. *Proceedings of ASME Turbo Expo 2013*, **GT2013-94941**.
- [27] Sridharan, K., Anderson, M. H., Cao, G., Jelinek, J. J., Firouzdar, V., and Allen, T. R., 2011. “Corrosion Testing of Materials in High Temperature Supercritical CarbonDioxide Environment”. *Proceedings of SCO₂ Power Cycle Sym-*

posium 2011.

- [28] Sarkar, J., 2009. “Second Law Analysis of Supercritical CO₂ Recompression Brayton Cycle”. *Energy*, **34**(9), pp. 1172–1178.
- [29] Poerner, M., Musgrove, G., and Beck, G., 2016. “Liquid CO₂ Formation Impact and Mitigation at the Inlet to A Supercritical CO₂ Compressor”. *Proceedings of ASME Turbo Expo 2016*, **GT2016-56513**.
- [30] Zangeneh, M., 1991. “A Compressible Three-dimensional Design Method for Radial and Mixed Flow Turbomachinery Blades”. *International Journal for Numerical Methods in Fluids*, **13**(5), pp. 599–624.
- [31] V6, T. S., 2016. “Advanced Design Technology Ltd, London, UK”. www.adtechnology.co.uk.
- [32] V6, T. S., 2016. “Advanced Design Technology Ltd, London, UK”. www.adtechnology.co.uk.
- [33] Zangeneh, M., Goto, A., and Takemura, T., 1996. “Suppression of Secondary Flows in A Mixed-flow Pump Impeller by Application of Three-dimensional Inverse Design Method: Part 1 Design and Numerical Validation”. *Journal of Turbomachinery*, **118**(3), pp. 536–543.
- [34] V6, T. S., 2016. “Advanced Design Technology Ltd, London, UK”. www.adtechnology.co.uk.
- [35] Menter, F. R., 1994. “Two-Equation Eddy-Viscosity Turbulence Models for Engineering Applications”. *AIAA Journal*, **32**(8), pp. 1598–1605.
- [36] Span, R., and Wagner, W., 1996. “A New Equation of State for Carbon Dioxide Covering the Fluid Region from the Triple-Point to 1100 K at Pressures up to 800 MPa”. *J. Phys. Chem. Ref. Data*, **25**(6), pp. 1509–1596.
- [37] INCONEL alloy 625 properties. Available from: www.specialmetals.com.
- [38] INCONEL alloy N06230 properties. Available from: www.specialmetals.com.
- [39] NIMONIC alloy PE16 properties. Available from: www.specialmetals.com.
- [40] PM2000 properties. Available from: www.matweb.com.